A Current-Control Strategy for Voltage-Source Inverters in Microgrids Based on H^∞ and Repetitive Control

Tomas Hornik and Qing-Chang Zhong, *Senior Member, IEEE*

***Abstract*—In this paper, a current-control strategy is proposed for voltage-source inverters in microgrids. The main objective of the proposed controller is to inject a clean sinusoidal current to the grid, even in the presence of nonlinear/unbalanced loads and/or grid-voltage distortions. The repetitive control technique is adopted because it can deal with a very large number of harmonics simultaneously. The proposed current controller consists of an internal model and a stabilizing compensator, which is designed by using the H^∞ control theory. It turns out that the stabilizing compensator may be simply an inductor. This leads to a very low total harmonic distortion (THD) and improved tracking performance. In order to demonstrate the improvement of performance, the proposed controller is compared with the traditional proportional–resonant, proportional–integral, and predictive deadbeat controllers. The control strategies are evaluated in the grid-connected mode with experiments under different scenarios: steady-state and transient responses without local loads, and steady-state responses with unbalanced resistive and nonlinear local loads. The proposed controller significantly outperforms the other control schemes in terms of the THD level, with the price of slightly slower dynamic responses.**

***Index Terms*—Current-controlled, grid-connected inverters, microgrids, repetitive control, total harmonic distortion (THD), voltage-source inverters (VSIs) .**

I. Introduction

MICROGRIDS are emerging as a consequence of rapidly growing distributed power generation systems (DPGS). Compared to a single DPGS, microgrids have more capacity and control flexibilities to fulfill system reliability and power quality requirements. A microgrid is normally operated in the grid-connected mode, but it is also expected to provide sufficient generation capacity, controls, and operational strategies to supply at least a part of the load after being disconnected from the public grid and to remain operational as a stand-alone (islanded) system [1]–[6]. As nonlinear and/or unbalanced loads can represent a high proportion of the total load in small-scale systems, the problem with power quality is a particular concern in microgrids [7]. The power quality assessment is mainly based on total harmonic distortion (THD) in voltages and currents. For both wind turbines and photovoltaic arrays connected to the utility grid, the maximum voltage and current THD allowed is 5% [8].

Traditionally, inverters used in microgrids behave as current sources when they are connected to the grid, and as voltage sources when they work autonomously [9]. Currently, most inverters in microgrids adopt the voltage-source inverter (VSI) topology [10]–[12] with a current controller to regulate the current injected into the grid. Current-controlled inverters have the advantages of the high-accuracy control of an instantaneous current, peak-current protection, overload rejection, and very good dynamics. The performance of the VSI depends on the quality of the applied current-control strategy and, in order to meet power quality requirements, inverters in microgrids should have very good capability in harmonic rejection.

Different strategies, e.g., proportional–integral (PI), proportional–resonant (PR), predictive deadbeat (DB), or hysteresis controllers have been proposed [13]. The PI control scheme in the synchronously rotating (d, q) reference frame is commonly used and can work well with balanced systems, but it cannot cope with unbalanced disturbance currents, which are common in microgrids. The PR control scheme in the stationary (α, β) reference frame is popular due to the capability of eliminating the steady-state error, while regulating sinusoidal signals, and the possible extension to compensate multiple harmonics. However, the resonant frequency in the controller has to be identical to the varying grid frequency in order to maintain good performance [13]. DB predictive control is widely used for current-error compensation and offers high performance for current-controlled VSIs. However, it is quite complicated and sensitive to system parameters [14], [15]. Hysteresis control is simple and brings fast responses, but it results in high and variable sampling frequencies, which leads to high current ripples, poor current quality, and difficulties in the output filter design. In order to obtain a fixed switching frequency, the complexity of the controller will be increased, if an adaptive band hysteresis controller is used [16], [17].

Repetitive control theory [18], regarded as a simple learning control method, provides an alternative to reduce the THD in voltages or currents. It is able to eliminate periodic errors in dynamic systems, according to the internal model principle [19], as it introduces high gains at the fundamental and all

Manuscript received July 1, 2010; revised October 3, 2010; accepted October 10, 2010. Date of current version May 13, 2011. The work of T. Hornik was supported by the Engineering and Physical Sciences Research Council, U.K. under the Doctoral Training Accounts (DTA) scheme, and the work of Q.-C. Zhong was supported by the Royal Academy of Engineering and the Leverhulme Trust with a Senior Research Fellowship (2009–2010). Recommended for publication by Associate Editor J. M. Guerrero.

T. Hornik is with the Department of Electrical Engineering & Electronics, The University of Liverpool, Liverpool, L69 3GJ, U.K. (e-mail: t.hornik@liv.ac.uk).

Q.-C. Zhong is with the Department of Aeronautical and Automotive Engineering, Loughborough University, Leicestershire, LE11 3TU, U.K. (e-mail: zhongqc@ieee.org).

Color versions of one or more of the figures in this paper are available online at http://ieeexplore.ieee.org.

Digital Object Identifier 10.1109/TPEL.2010.2089471

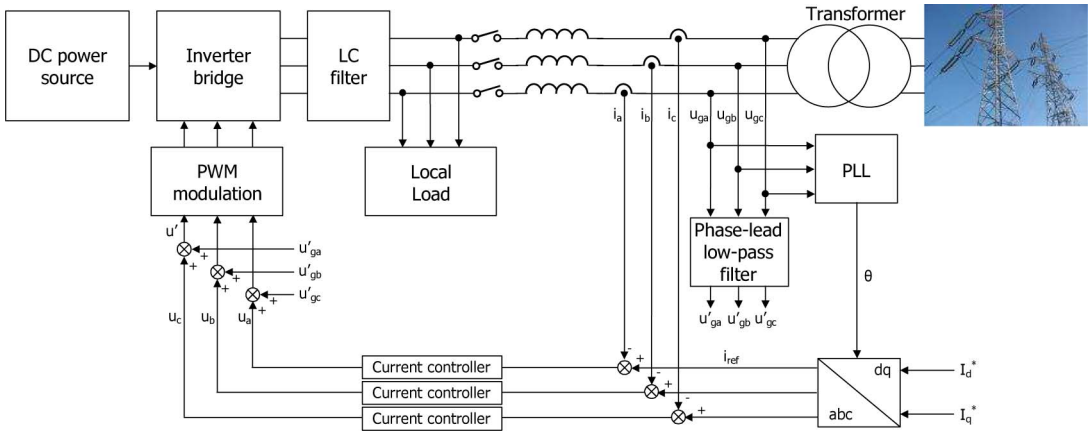

Fig. 1. Block diagram of a current-controlled inverter in the natural frame using H^∞ and repetitive control techniques.

harmonic frequencies of interest. The internal model is infinite-dimensional and can be obtained by connecting a delay line into a feedback loop. Such a closed-loop system can deal with a very large number of harmonics simultaneously. It has been successfully applied to constant-voltage constant-frequency pulsewidth modulation (PWM) inverters [20], [21], grid-connected inverters [22], [23], and active filters [24], [25]. However, these are mainly used in the form of voltage controllers except the one in [23].

In this paper, a current controller is proposed for inverters in microgrids based on H^∞ and repetitive control techniques. The voltage controller proposed in [22] is replaced with a current repetitive controller and then experimentally validated. The attention is paid to improving power quality and tracking performance, and considerably reducing the complexity of the controller design. The model of the plant is reduced to single-input-single-output for the repetitive control design. As a consequence, the design becomes much simpler and the stability evaluation becomes easier. The grid voltage in the grid-connected mode or the reference voltage in the stand-alone mode is feed-forwarded and added onto the output of the current controller. This considerably facilitates the design of the controller and the operation of the system. Moreover, a frequency-adaptive mechanism proposed in [26] is implemented so that the controller can cope with grid-frequency variations. This mechanism allows the controller to maintain very good tracking performance over a wide range of grid frequencies. As a result, the power quality and tracking performance are considerably improved and the achieved current THD is less than 1%. The strategy allows the local loads connected to the microgrid to be unbalanced and/or nonlinear because the current under control is the current flowing to the grid and the microgrid (load) voltage is feed-forwarded from the grid or set by the reference. In order to demonstrate the improvement of performance, experiments are carried out using the proposed controller and compared with the traditional PR, PI, and predictive DB controllers.

The overall structure of the system is described in Section II, followed by the current-controller design using the H^∞ control theory in Section III. In Section IV, the experimental setup is briefly described and experimental results are presented and discussed. Conclusions are made in Section V.

II. Description of the Proposed System

The proposed control system, as shown in Fig. 1, adopts an individual controller for each phase in the natural frame. This is also called abc control. The system is equipped with a neutral point controller proposed in [27] to maintain a balanced neutral point (not shown nor discussed in this paper). As the neutral point circuit is a combination of the split dc link and the additional neutral leg topology, the control of the neutral leg is decoupled from the control of the three-phase inverter and has no effect on its performance [27]. The proposed system consists of a current loop including a repetitive controller so that the current injected into the grid could track the reference current $i_{\rm ref}$, which is generated from the d, q-current references I_d^* and I_q^* using the $dq \rightarrow abc$ transformation in this paper (three separate current references can be used instead). A phase-locked loop is used to provide the phase information of the grid voltage, which is needed to generate $i_{\rm ref}$. The real power and reactive power exchanged with the grid are determined by I_d^* and I_q^* (and, of course, the grid voltage). The inverter is assumed to be powered by a constant dc power source and, hence, no controller is needed to regulate the dc-link voltage (otherwise, a controller can be introduced to regulate the dc-link voltage and to generate I_d^* accordingly).

When the references I_d^* and I_q^* are all equal to 0, the generated voltage should be equal to the grid voltage, i.e., the inverter should be synchronized with the grid and the circuit breaker could be closed at any time if needed. In order to achieve this, the grid voltages (u_{ga}, u_{gb}, and u_{gc}) are feed-forwarded and added to the output of the repetitive current controller via a phase-lead low-pass filter

$$F(s) = \frac{33(0.05s+1)}{(s+300)(0.002s+1)}$$

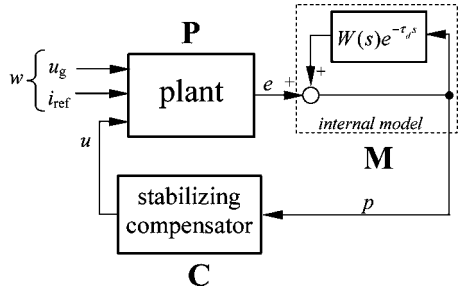

Fig. 2. Block diagram of the H^∞ repetitive current-control scheme.

which has a gain slightly higher than 1 and a phase lead at the fundamental frequency. It is introduced to compensate the phase shift and gain attenuation caused by the computational delay, PWM modulation, the inverter bridge, and the *LC* filter (otherwise, it could be a unity gain). It also attenuates the harmonics in the feed-forwarded grid voltages and improves the dynamics during grid-voltage fluctuations [13]. This filter could be designed analytically, but it can be chosen easily according to the principles just mentioned. The accuracy does not seriously affect the performance because the main objective is to control the grid current not the microgrid voltage. Another advantage of this scheme is that it does not affect the independence of each phase. After the circuit breaker is closed, there should be no current flowing to the grid until the current references are changed to be nonzero. When the inverter generates power, the repetitive current controller makes appropriate contributions on top of the feed-forwarded grid voltages. The output current to the grid is used as feedback and the microgrid voltage is maintained using the feed-forwarded grid voltage (open-loop control) (see Fig. 1). Such an arrangement allows nonlinear or unbalanced loads to be connected to the microgrid while maintaining the grid currents to be balanced and clean, which minimizes the impact of microgrids on the public grid.

III. Design of the Repetitive Current Controller

In this section, the current controller is designed based on the H^∞ and repetitive control techniques, after establishing the inverter model. The main objective of the H^∞ repetitive current controller is to inject a clean and balanced current to the grid, even in the presence of nonlinear and/or unbalanced loads with grid-voltage distortions. The block diagram of the H^∞ repetitive current-control scheme is shown in Fig. 2, where P is the transfer function of the plant, C is the stabilizing compensator to be designed, and M is the transfer function of the internal model. The stabilizing compensator C and internal model M are the two components of the proposed controller. The stabilizing compensator C, designed by solving a weighted sensitivity H^∞ problem [28], assures the exponential stability of the entire system. Hence, the tracking error e between the current reference and the current injected to the grid converges to a small steady-state error [29]. The internal model M is a local positive feedback of a delay line cascaded with a low-pass filter $W(s)$. The external signal w contains both the grid voltage u_g and the current reference $i_{\rm ref}$, which are assumed to be periodic with a fundamental frequency of 50 Hz.

A. State-Space Model of the Plant P

The considered plant consists of the inverter bridge, an *LC* filter (L_f and C_f), and a grid interface inductor L_g (see the single-phase diagram of the system shown in Fig. 3). The *LC* filter and the grid-interface inductor form an *LCL* filter and the filter inductors are modeled with series resistance. The circuit breaker S_C is needed during the synchronization and shut down procedure. The PWM block together with the inverter bridge are modeled by using an average voltage approach with the limits of the available dc-link voltage [22] so that the fundamental component of u_f is equal to $u' = u + u'_g$. As a result, the PWM block and the inverter bridge can be ignored when designing the controller. At the same time, the feed-forwarded grid voltage u'_g actually provides a base voltage for the microgrid. The same voltage appears on both sides of the *LCL* filter and can be regarded as a voltage disturbance added on the capacitor. It does not affect the controller design and can be ignored during the design process. The only contribution needs to be considered during the design process is the output u of the repetitive current controller (see Figs. 1 and 2). This observation is very important for the controller design. It is worth noting that the local loads are connected to the microgrid at point u_o (not at the grid u_g). This allows the loads to be powered by the dc source when the microgrid is disconnected from the grid (when S_c is OFF). It also allows that the (microgrid) voltage for the loads could be cleaner than the grid voltage and that the impact of nonlinear/unbalanced local loads on the grid could be minimized. The local loads will not be considered at the design stage, but will be added at the experimental stage to test the robustness of the controller designed. This is practical because the load could be arbitrary.

The currents of the two inductors and the voltage of the capacitor are chosen as state variables $x = [\, i_1 \quad i_2 \quad u_c \,]^T$. The external input is $w = [\, u_g \quad i_{\rm ref} \,]^T$ and the control input is u. The output signal from the plant P is the tracking error $e = i_{\rm ref} - i_2$, i.e., the difference between the current reference and the current injected into the grid. The plant P can then be described by the state equation

$$\dot{x} = Ax + B_1 w + B_2 u \tag{1}$$

and the output equation

$$y = e = C_1 x + D_1 w + D_2 u \tag{2}$$

with

$$A = \begin{bmatrix} -\dfrac{R_f + R_d}{L_f} & \dfrac{R_d}{L_f} & -\dfrac{1}{L_f} \\ \dfrac{R_d}{L_g} & -\dfrac{R_g + R_d}{L_g} & \dfrac{1}{L_g} \\ \dfrac{1}{C_f} & -\dfrac{1}{C_f} & 0 \end{bmatrix}$$

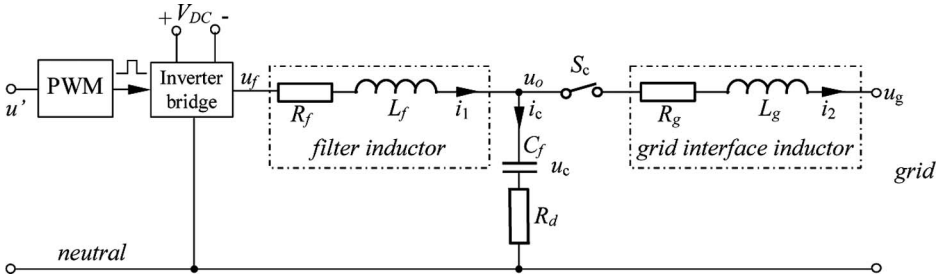

Fig. 3. Single-phase representation of the plant P (the inverter).

$$B_1 = \begin{bmatrix} 0 & 0 \\ -\dfrac{1}{L_g} & 0 \\ 0 & 0 \end{bmatrix} \qquad B_2 = \begin{bmatrix} \dfrac{1}{L_f} \\ 0 \\ 0 \end{bmatrix}$$

$$C_1 = [\,0 \quad -1 \quad 0\,] \qquad D_1 = [\,0 \quad 1\,] \qquad D_2 = 0.$$

The corresponding plant transfer function is then $P = [\,D_1 \quad D_2\,] + C_1(sI - A)^{-1}\,[\,B_1 \quad B_2\,]$. In the sequel, the following notation will be used for transfer functions:

$$P = \left[\begin{array}{c|cc} A & B_1 & B_2 \\ \hline C_1 & D_1 & D_2 \end{array}\right]. \tag{3}$$

B. Internal Model M

The internal model M, as shown in Fig. 2, is infinite-dimensional and consists of a low-pass filter $W(s) = \omega_c/(s + \omega_c)$ cascaded with a delay line $e^{-\tau_d s}$. It is capable of generating periodic signals of a given fundamental period τ_d; therefore, it is capable of tracking periodic references and rejecting periodic disturbances having the same period. The delay time τ_d should be slightly less than the fundamental period τ [22], [29], and can be chosen as

$$\tau_d = \tau - \frac{1}{\omega_c} \tag{4}$$

where ω_c is the cutoff frequency of the low-pass filter W. This allows the repetitive control scheme to cover a wide range of harmonics (see the plot of poles of the internal model depicted in [22]). However, when the grid frequency f varies, the performance of the internal model is degraded. In order to maintain the tracking performance of the controller, the frequency-adaptive mechanism proposed in [26] is used to dynamically change the cutoff frequency ω_c of the low-pass filter. This is able to move the poles of the internal model accordingly. When the change of the grid frequency is severe, it is necessary to change τ_d as well.

C. Formulation of the Standard H^∞ Problem

In order to guarantee the stability of the system, an H^∞ control problem, as shown in Fig. 4, is formulated to minimize the H^∞ norm of the transfer function $T_{\tilde{z}\tilde{w}} = \mathcal{F}_l(\tilde{P}, C)$ from $\tilde{w} = [\,v \quad w\,]^T$ to $\tilde{z} = [\,z_1 \quad z_2\,]^T$, after opening the local positive-feedback loop of the internal model and introducing

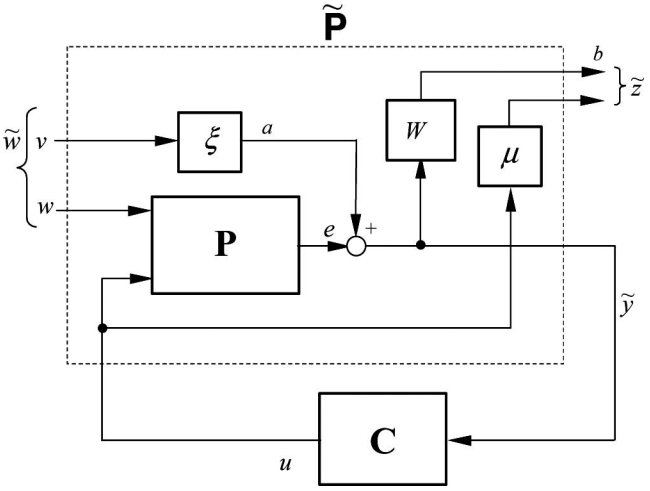

Fig. 4. Formulation of the H^∞ control problem.

weighting parameters ξ and μ. The closed-loop system can be represented as

$$\begin{bmatrix} \tilde{z} \\ \tilde{y} \end{bmatrix} = \tilde{P} \begin{bmatrix} \tilde{w} \\ u \end{bmatrix}, \quad u = C\tilde{y}$$

where $\tilde{P}$ is the extended plant and C is the controller to be designed. The extended plant $\tilde{P}$ consists of the original plant P together with the low-pass filter W and weighting parameters ξ and μ. The additional parameters ξ and μ are added to provide more freedom in design. Moreover, the MATLAB *hinfsyn* algorithm, which solves the standard H^∞ problem needs D_{12} to have full column rank and D_{21} to have full row rank, respectively.

Assume that W is realized as

$$W = \left[\begin{array}{c|c} A_w & B_w \\ \hline C_w & 0 \end{array}\right] = \left[\begin{array}{c|c} -\omega_c & \omega_c \\ \hline 1 & 0 \end{array}\right].$$

From Fig. 4, the following equations can be obtained:

$$\tilde{y} = e + \xi v = \xi v + \left[\begin{array}{c|cc} A & B_1 & B_2 \\ \hline C_1 & D_1 & D_2 \end{array}\right] \begin{bmatrix} w \\ u \end{bmatrix} \tag{5}$$

$$= \left[\begin{array}{c|ccc} A & 0 & B_1 & B_2 \\ \hline C_1 & \xi & D_1 & D_2 \end{array}\right] \begin{bmatrix} v \\ w \\ u \end{bmatrix}$$

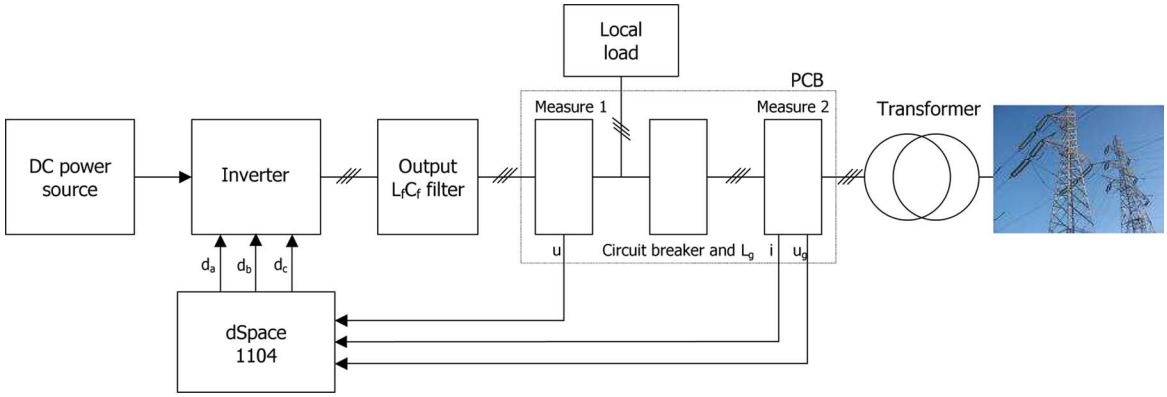

Fig. 5. Block diagram of the experimental setup.

$$z_1 = W(e + \xi v) = \left[\begin{array}{cc|ccc} A & 0 & 0 & B_1 & B_2 \\ B_w C_1 & A_w & B_w \xi & B_w D_1 & B_w D_2 \\ \hline 0 & C_w & 0 & 0 & 0 \end{array}\right] \begin{bmatrix} v \\ w \\ u \end{bmatrix} \quad (6)$$

$$z_2 = \mu u. \quad (7)$$

Combining (5)–(7), the realization of the extended plant is then obtained as

$$\tilde{P} = \left[\begin{array}{cc|cc:c} A & 0 & 0 & B_1 & B_2 \\ B_w C_1 & A_w & B_w \xi & B_w D_1 & B_w D_2 \\ \hline 0 & C_w & 0 & 0 & 0 \\ 0 & 0 & 0 & 0 & \mu \\ \hdashline C_1 & 0 & \xi & D_1 & D_2 \end{array}\right]. \quad (8)$$

The stabilizing controller C can be calculated using the well-known results on H^∞ controller design [30] for the extended plant $\tilde{P}$.

D. Evaluation of the System Stability

According to [22] and [29], the closed-loop system in Fig. 2 is exponentially stable, if the closed-loop system from Fig. 4 is stable and its transfer function from a to b, denoted T_{ba}, satisfies $\|T_{ba}\|_\infty < 1$. Assume that the state-space realization of the controller is

$$C = \left[\begin{array}{c|c} A_c & B_c \\ \hline C_c & D_c \end{array}\right].$$

Note that the central optimal controller obtained from the H^∞ design is always strictly proper. However, after controller reduction, the reduced controller may not be strictly proper (and hence the D_c may not be 0). The realization of the transfer function from a to b, assuming that $w = 0$ and noting that $D_2 = 0$, can be found as follows:

$$T_{ba} = \left(1 - \left[\begin{array}{c|c} A & B_2 \\ \hline C_1 & 0 \end{array}\right] C\right)^{-1} W = \left[\begin{array}{ccc|c} A + B_2 D_c C_1 & B_2 C_c & B_2 D_c C_w & 0 \\ B_c C_1 & A_c & B_c C_w & 0 \\ 0 & 0 & A_w & B_w \\ \hline C_1 & 0 & C_w & 0 \end{array}\right].$$

Once the controller C is obtained, the stability of the system can be verified by checking $\|T_{ba}\|_\infty$.

IV. Experimental Validation

A. Experimental Setup

The experimental setup, shown in Fig. 5, consists of an inverter board, a three-phase *LC* filter, a three-phase grid interface inductor, a board consisting of voltage and current sensors, a step-up transformer, a dSPACE DS1104 R&D controller board with ControlDesk software, and MATLAB Simulink/SimPower software package. The inverter board consists of two independent three-phase inverters and has the capability to generate PWM voltages from a constant dc-voltage source. 42 V was used for safety reasons. The first inverter is used to generate three-phase voltages and the second one is used to control the neutral point [27]. The generated three-phase voltage is connected to the grid via a controlled circuit breaker and a step-up transformer. The grid voltage and the current injected into the grid are measured for control purposes. The sampling frequency of the controller is 5 kHz and the PWM switching frequency is 12 kHz. A Yokogawa WT1600 power analyzer is used to measure THD (up to the 31st harmonic component). The parameters of the system are given in Table I.

B. H^∞ Controller Design

The low-pass filter W is chosen according to [26] as

$$W = \left[\begin{array}{c|c} -2550 & 2550 \\ \hline 1 & 0 \end{array}\right]$$

TABLE I
PARAMETERS OF THE INVERTER

Parameter	Value	Parameter	Value
L_f	$150\mu H$	R_f	0.045Ω
L_g	$450\mu H$	R_g	0.135Ω
C_f	$22\mu F$	R_d	1Ω

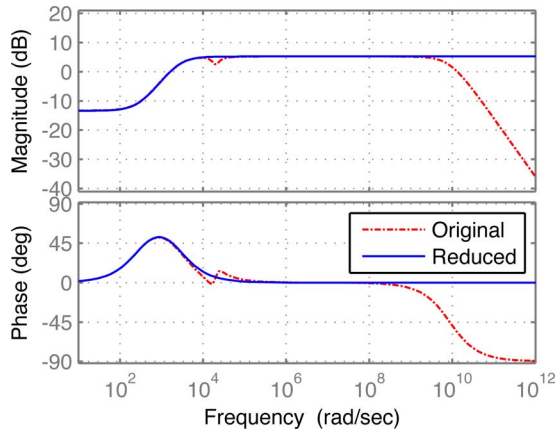

Fig. 6. Bode plots of the original and reduced controllers.

for $f = 50$ Hz. The weighting parameters are chosen to be $\xi = 100$ and $\mu = 0.26$. Using the MATLAB *hinfsyn* algorithm, the H^∞ controller C that nearly minimizes the H^∞ norm of the transfer matrix from $\tilde{w}$ to $\tilde{z}$ is obtained as

$$C(s) = \frac{13110139652.7671(s+300.8)(s^2+9189s+4.04\times10^8)}{(s+7.39\times10^9)(s+2550)(s^2+1.236\times10^4 s+3.998\times10^8)}.$$

The factor $s + 7.39 \times 10^9$ in the denominator can be approximated by the constant 7.39×10^9 without causing any noticeable performance change [29]. The poles and zeros that are close to each other can be canceled as well, which makes the controller less sensitive to component parameters. The resulting reduced controller is

$$C(s) = \frac{1.774(s+300.8)}{s+2550} \doteq W(s)C_{PD}(s)$$

with

$$C_{PD}(s) = 0.21 + 0.696\times10^{-3}s$$

which is a 0.696-mH inductor with an internal resistance of $0.21\,\Omega$. The current controller is simply an inductor cascaded with the internal model (in a rearranged form), which transforms the current difference into a voltage signal.

The Bode plots of the original and reduced controllers in the continuous time domain are shown in Fig. 6 for comparison. There is little difference at low frequencies. The Bode plots in the discrete time domain are almost identical, for the sampling frequency of 5 kHz used for implementation. Using the MATLAB c2d (ZOH) algorithm, the discretized controller can be obtained as

$$C(z) = \frac{1.774(z-0.9529)}{z-0.6005}.$$

The resulting $\|T_{ba}\|_\infty$ is 0.4555 and, hence, the closed-loop system is stable. Actually, the robustness of the system is very good.

C. Experimental Results

The proposed controller is compared with the traditional PR, PI, and predictive DB controllers designed according to [13]. All controllers are implemented in the natural frame shown in Fig. 1. The control strategies are evaluated in the grid-connected mode under three different scenarios: without local loads, with unbalanced resistive local loads, and with nonlinear local loads.

1) Steady-State Responses—Without Local Loads: The current reference I_d^* was set at 3 A and I_q^* was set at 0. This corresponds to the unity power factor. Since there is no local load included in the experiment, all generated active power was injected into the grid via the step-up transformer. The grid output currents i_A, reference current $i_{\rm ref}$, and the corresponding current tracking error e_i in the steady state with the different controllers are shown in the left column of Fig. 7, and their harmonic spectra are shown in the left column of Fig. 8. The corresponding recorded THD are shown in Table II. The H^∞ repetitive controller shows much better harmonics rejection and tracking performance than the other controllers. It is worth mentioning that the quality of the output current is better than that of the grid voltage.

2) Steady-State Responses—With Unbalanced Resistive Local Loads: In this experiment, unbalanced resistive local loads were connected to the inverter ($R_A = 12\,\Omega$, $R_B = \infty$, and $R_C = 12\,\Omega$). The grid output current reference I_d^* was set at 2 A (after connecting the inverter to the grid). The reactive power was set at 0 VAR ($I_q^* = 0$). The output current i_A, reference current $i_{\rm ref}$, and the corresponding current tracking error e_i in the steady state with the different controllers are shown in the middle column of Fig. 7, and their harmonic spectra are shown in the middle column of Fig. 8. The corresponding recorded THD are shown in Table III. The proposed controller performs much better than the other controllers. The PI controller demonstrated difficulties in coping with the unbalanced loads and the tracking error was increased. The tracking performance of the other three controllers remains satisfactory.

3) Steady-State Responses—With Balanced Nonlinear Local Load: In this experiment, a nonlinear load (a three-phase uncontrolled rectifier loaded with an LC filter $L = 150\,\mu$H, $C = 1000\,\mu$F, and a resistor $R = 20\,\Omega$) was connected to the inverter. The grid output current reference I_d^* was set at 2 A (after connecting the inverter to the grid). The reactive power was set at 0 VAR ($I_q^* = 0$). The output current i_A, reference current $i_{\rm ref}$, and the corresponding current tracking error e_i in the steady state for the different controllers are shown in the right column of Fig. 7, and their harmonic spectra are shown in the right column of Fig. 8. The corresponding recorded THD are shown in Table IV. The H^∞ repetitive controller significantly

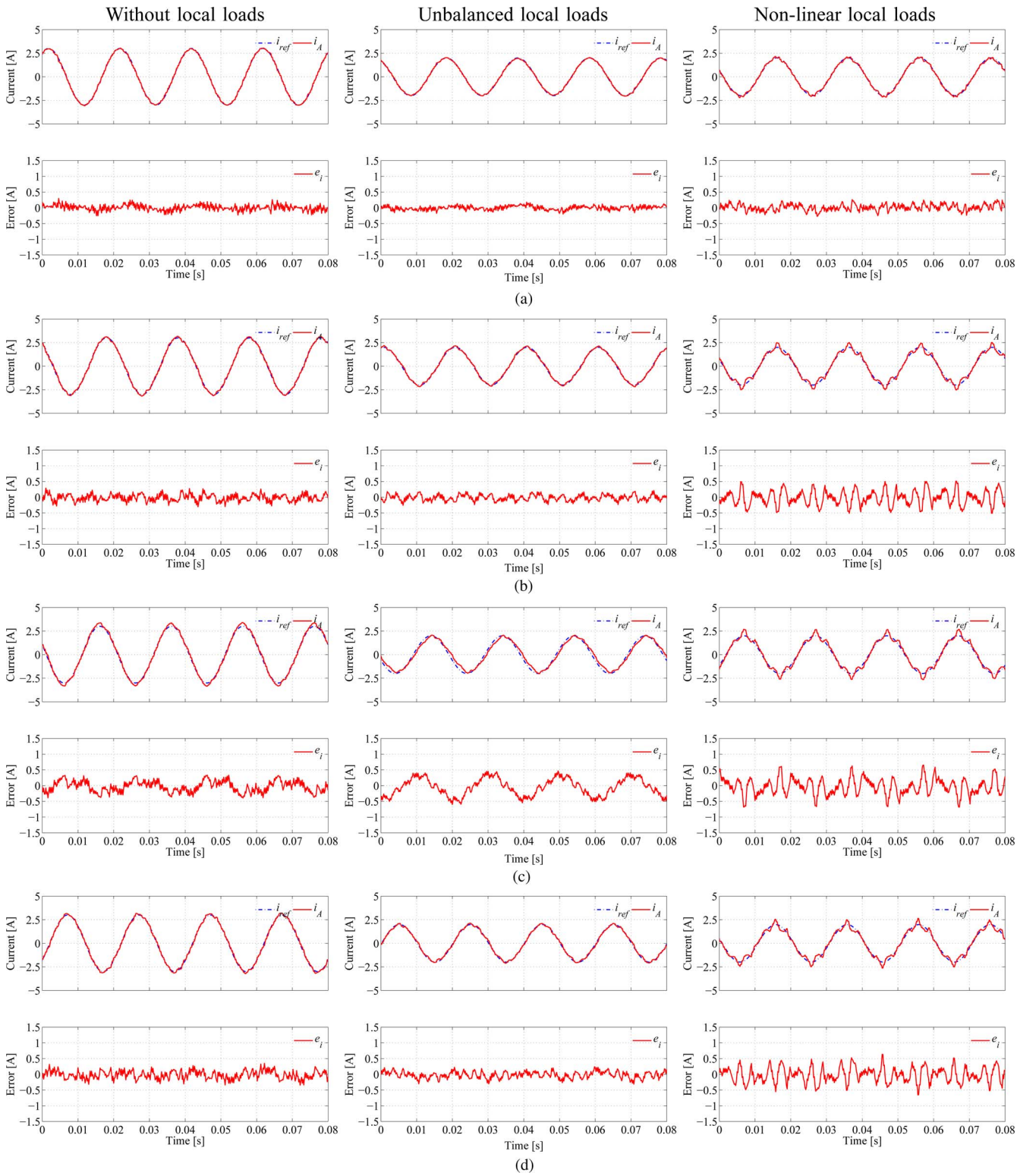

Fig. 7. Steady-state responses. Without local loads (left column), with unbalanced resistive local loads (middle column), and with nonlinear local loads (right column). (a) H^∞ repetitive controller. (b) PR controller. (c) PI controller. (d) DB controller.

outperformed the other three controllers, as the corresponding THD is approximately one-third of the others and the tracking error e_i remains almost unchanged with respect to earlier experiments.

D. Transient Responses

In order to compare their transient performance, a step change in the current reference I_d^* from 2–3 A was applied (while keeping $I_q^* = 0$). All generated active power was again injected into

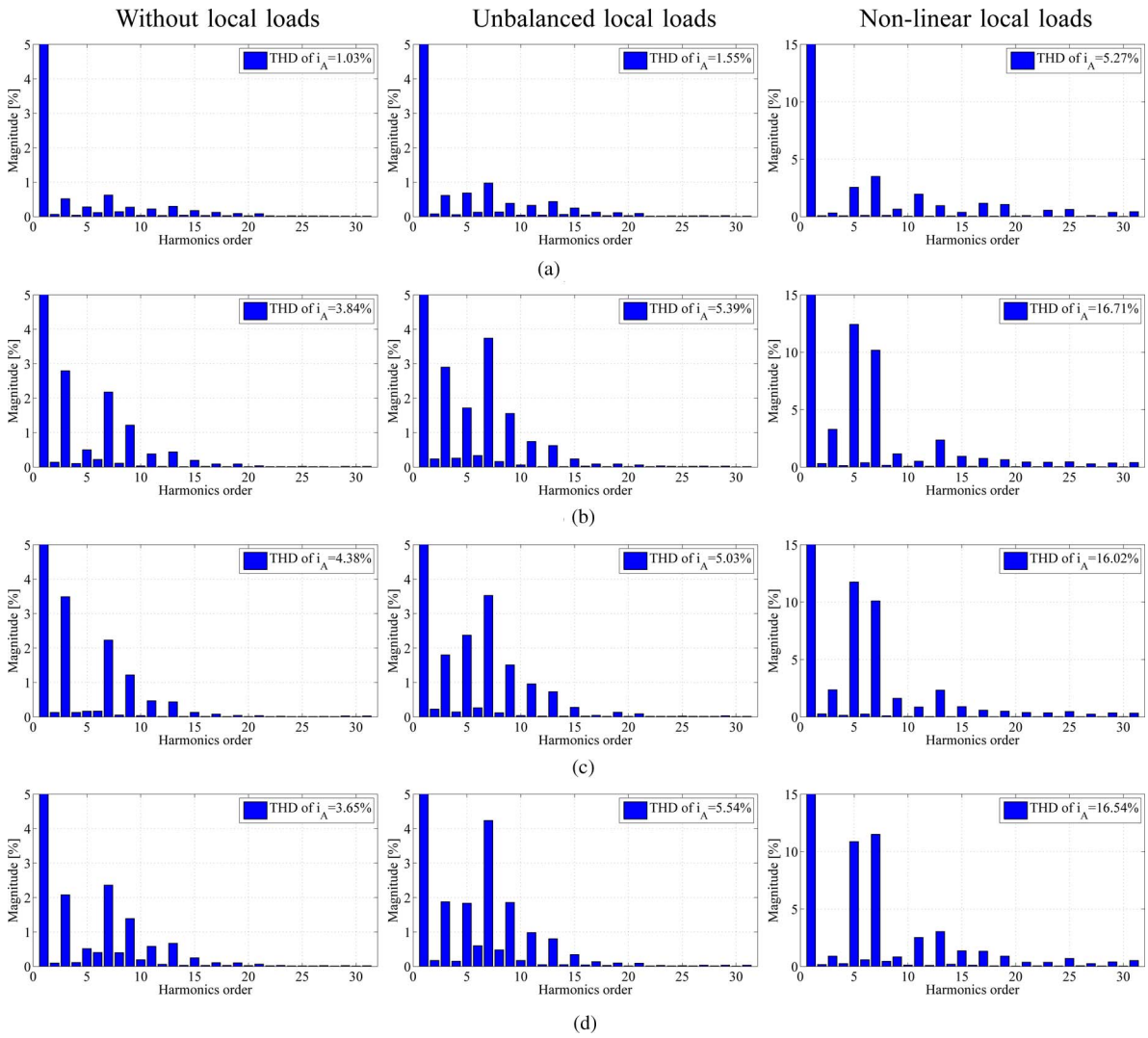

Fig. 8. Spectra of the current sent to the grid. without local loads (left column), with unbalanced resistive local loads (middle column), and with nonlinear local loads (right column). (a) H^∞ repetitive controller. (b) PR controller. (c) PI controller. (d) DB controller.

TABLE II
THD OF THE CURRENTS SENT TO THE GRID: WITHOUT LOCAL LOADS

Controller	Current i_A THD [%]	Grid voltage v_{gA} THD [%]
H^∞ repetitive	1.03	1.57
PR	3.84	1.45
PI	4.38	1.52
DB	3.65	1.61

TABLE III
THD OF THE CURRENTS SENT TO THE GRID: WITH UNBALANCED RESISTIVE LOCAL LOADS

Controller	Current i_A THD [%]	Grid Voltage v_{gA} THD [%]
H^∞ Repetitive	1.55	1.59
PR	5.39	1.45
PI	5.03	1.48
DB	5.54	1.52

TABLE IV
THD OF THE CURRENTS SENT TO THE GRID: WITH NONLINEAR LOCAL LOADS

Controller	Current i_A THD [%]	Grid voltage v_{gA} THD [%]
H^∞ repetitive	5.27	1.6
PR	16.71	1.47
PI	16.02	1.41
DB	16.54	1.49

the grid via a step-up transformer. The transient response of the output current i_A, reference current $i_{\rm ref}$, and the corresponding current tracking error e_i are shown in Fig. 9 for the different controllers adopted. The experimental results indicate that the DB controller shows the fastest dynamics. The H^∞ repetitive controller is the slowest with comparison to the other controllers. It took about five cycles to settle down. This reflects the inherent property of the repetitive control, which is the price paid for the low THD in the currents.

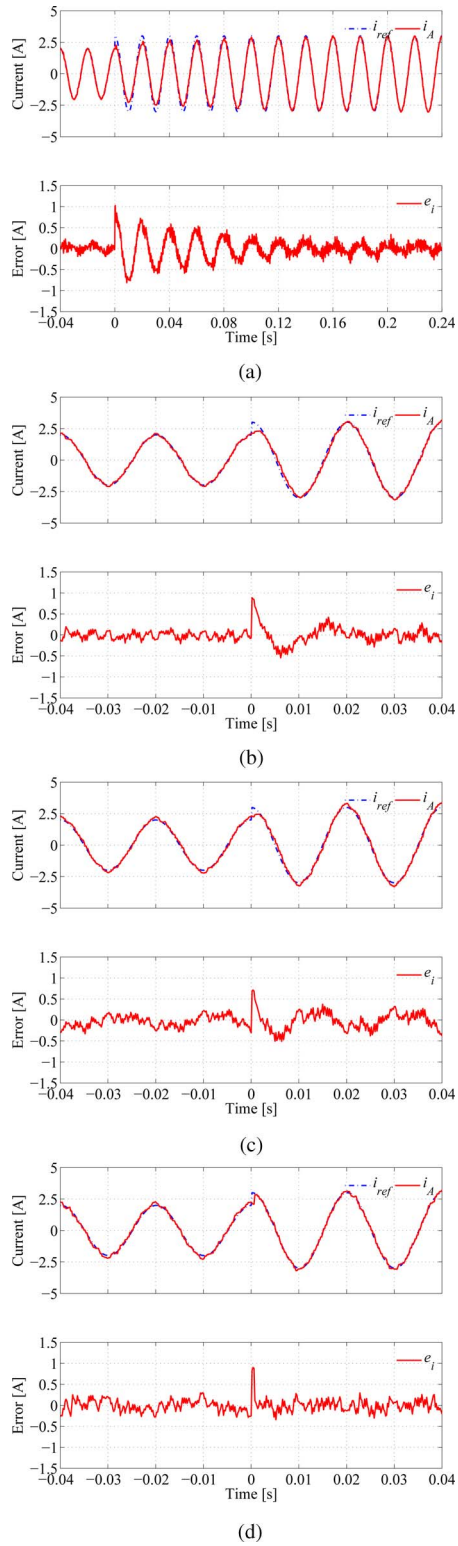

Fig. 9. Transient responses of the grid-connected inverter without local loads. (a) H^∞ repetitive controller. (b) PR controller. (c) PI controller. (d) DB controller.

V. Conclusion

The H^∞ repetitive control strategy has been applied to the design of a current controller for grid-connected VSI. The proposed controller is compared with the traditional PR, PI, and predictive DB controllers, all implemented in the natural frame with the main focus on harmonics distortion and tracking performance. The H^∞ repetitive controller offers significant improvement over the conventional PI, PR, and DB controllers and leads to very low THD for the output current, even in the presence of nonlinear/unbalanced loads and/or grid-voltage distortion. The price paid for this is its relatively slow dynamics (the slightly more complex calculation and design are no longer a main issue because of the advances in digital signal processing and controller design).

References

[1] N. Hatziargyriou, H. Asano, R. Iravani, and C. Marnay, "Microgrids," *IEEE Power Energy Mag.*, vol. 5, no. 4, pp. 78–94, Jul./Aug. 2007.

[2] F. Katiraei, R. Iravani, N. Hatziargyriou, and A. Dimeas, "Microgrids management," *IEEE Power Energy Mag.*, vol. 6, no. 3, pp. 54–65, May/Jun. 2008.

[3] C. Xiarnay, H. Asano, S. Papathanassiou, and G. Strbac, "Policymaking for microgrids," *IEEE Power Energy Mag.*, vol. 6, no. 3, pp. 66–77, May/Jun. 2008.

[4] Y. Mohamed and E. F. El-Saadany, "Adaptive decentralized droop controller to preserve power sharing stability of paralleled inverters in distributed generation microgrids," *IEEE Trans. Power Electron.*, vol. 23, no. 6, pp. 2806–2816, Nov. 2008.

[5] Y. W. Li and C.-N. Kao, "An accurate power control strategy for power-electronics-interfaced distributed generation units operating in a low-voltage multibus microgrid," *IEEE Trans. Power Electron.*, vol. 24, no. 12, pp. 2977–2988, Dec. 2009.

[6] C.-L. Chen, Y. Wang, J.-S. Lai, Y.-S. Lee, and D. Martin, "Design of parallel inverters for smooth mode transfer microgrid applications," *IEEE Trans. Power Electron.*, vol. 25, no. 1, pp. 6–15, Jan. 2010.

[7] M. Prodanovic and T. C. Green, "High-quality power generation through distributed control of a power park microgrid," *IEEE Trans. Ind. Electron.*, vol. 53, no. 5, pp. 1471–1482, Oct. 2006.

[8] *IEEE Recommended Practices and Requirements for Harmonic Control in Electrical Power Systems*, IEEE Standard 519-1992, Apr. 1993.

[9] J. M. Guerrero, J. C. Vasquez, J. Matas, M. Castilla, and L. G. de Vicuna, "Control strategy for flexible microgrid based on parallel line-interactive UPS systems," *IEEE Trans. Ind. Electron.*, vol. 56, no. 3, pp. 726–736, Mar. 2009.

[10] Y. A.-R. Mohamed and E. F. El-Saadany, "Adaptive discrete-time grid-voltage sensorless interfacing scheme for grid-connected dg-inverters based on neural-network identification and deadbeat current regulation," *IEEE Trans. Power Electron.*, vol. 23, no. 1, pp. 308–321, Jan. 2008.

[11] G. Shen, D. Xu, L. Cao, and X. Zhu, "An improved control strategy for grid-connected voltage source inverters with an LCL filter," *IEEE Trans. Power Electron.*, vol. 23, no. 4, pp. 1899–1906, Jul. 2008.

[12] I. J. Gabe, V. F. Montagner, and H. Pinheiro, "Design and implementation of a robust current controller for VSI connected to the grid through an lcl filter," *IEEE Trans. Power Electron.*, vol. 24, no. 6, pp. 1444–1452, Jun. 2009.

[13] A. Timbus, M. Liserre, R. Teodorescu, P. Rodriguez, and F. Blaabjerg, "Evaluation of current controllers for distributed power generation systems," *IEEE Trans. Power Electron.*, vol. 24, no. 3, pp. 654–664, Mar. 2009.

[14] Y. A.-R. I. Mohamed and E. F. El-Saadany, "Robust high bandwidth discrete-time predictive current control with predictive internal model—A unified approach for voltage-source PWM converters," *IEEE Trans. Power Electron.*, vol. 23, no. 1, pp. 126–136, Jan. 2008.

[15] J. C. Moreno, J. M. E. Huerta, R. G. Gil, and S. A. Gonzalez, "A robust predictive current control for three-phase grid-connected inverters," *IEEE Trans. Ind. Electron.*, vol. 56, no. 6, Jun. 2009.

[16] V. George and M. K. Mishra, "Design and analysis of user-defined constant switching frequency current-control-based four-leg DSTATCOM," *IEEE Trans. Power Electron.*, vol. 24, no. 9, pp. 2148–2158, Sep. 2009.

[17] C. N.-M. Ho, V. S. P. Cheung, and H. S.-H. Chung, "Constant-frequency hysteresis current control of grid-connected VSI without bandwidth control," *IEEE Trans. Power Electron.*, vol. 24, no. 11, pp. 2484–2495, Nov. 2009.

[18] S. Hara, Y. Yamamoto, T. Omata, and M. Nakano, "Repetitive control system: a new type servo system for periodic exogenous signals," *IEEE Trans. Automatic Control*, vol. 33, no. 7, pp. 659–668, Jul. 1988.

[19] B. A. Francis and W. M. Wonham, "The internal model principle for linear multivariable regulators," *Appl. Math. & Optim.*, vol. 2, no. 2, pp. 170–194, Dec. 1975.
[20] B. Zhang, D. Wang, K. Zhou, and Y. Wang, "Linear phase lead compensation repetitive control of a CVCF PWM inverter," *IEEE Trans. Ind. Electron.*, vol. 55, no. 4, pp. 1595–1602, Apr. 2008.
[21] K. Zhou, D. Wang, B. Zhang, and Y. Wang, "Plug-in dual-mode-structure repetitive controller for CVCF PWM inverters," *IEEE Trans. Ind. Electron.*, vol. 56, no. 3, pp. 784–791, Mar. 2009.
[22] G. Weiss, Q.-C. Zhong, T. C. Green, and J. Liang, "H^∞ repetitive control of DC-AC converters in microgrids," *IEEE Trans. Power Electron.*, vol. 19, no. 1, pp. 219–230, Jan. 2004.
[23] K. Toyama, H. Ohtake, S. Matsuda, S. Kobayashi, M. Morimoto, and H. Sugimoto, "Repetitive control of current for residential photovoltaic generation system," in *Proc. 26th Annu. Conf. IEEE Ind. Electron. Soc.*, 2000, vol. 2, pp. 741–745.
[24] A. Garcia-Cerrada, O. Pinzon-Ardila, V. Feliu-Batlle, P. Roncero-Sanchez, and P. Garcia-Gonzalez, "Application of a repetitive controller for a three-phase active power filter," *IEEE Trans. Power Electron.*, vol. 22, no. 1, pp. 237–246, Jan. 2007.
[25] G. Escobar, P. G. Hernandez-Briones, P. R. Martinez, M. Hernandez-Gomez, and R. E. Torres-Olguin, "A repetitive-based controller for the compensation of harmonic components," *IEEE Trans. Ind. Electron.*, vol. 55, no. 8, pp. 3150–3158, Aug. 2008.
[26] T. Hornik and Q.-C. Zhong, "H^∞ repetitive voltage control of grid-connected inverters with frequency adaptive mechanism," *IET Power Electron.*, vol. 3, no. 6, pp. 925–935, Nov. 2010.
[27] Q.-C. Zhong, J. Liang, G. Weiss, C. Feng, and T. C. Green, "H^∞ control of the neutral point in four-wire three-phase DC-AC converters," *IEEE Trans. Ind. Electron.*, vol. 53, no. 5, pp. 1594–1602, Oct. 2006.
[28] G. Weiss, D. Neuffer, and D. H. Owens, "A simple scheme for internal model based control," in *Proc. UKACC Int. Conf. Control*, Sep. 1998, pp. 630–634.
[29] G. Weiss and M. Hafele, "Repetitive control of MIMO systems using H^∞ design," *Automatica*, vol. 35, pp. 1185–1199, 1999.
[30] K. Zhou, J. C. Doyle, and K. Glover, *Robust and optimal control*. Upper Saddle River, NJ: Prentice Hall, 1996.

Tomas Hornik received the Diploma degree in electrical engineering from Technical College V Uzlabine, Prague, in 1991, and the B.Eng. and Ph.D. degrees in electrical engineering and electronics from the University of Liverpool, Liverpool, U.K., in 2007 and 2010, respectively.

He had been a System Engineer for more than ten years involved in commissioning and software design in power generation and distribution, control systems for central heating systems, and building management systems. He is currently a Postdoctoral Researcher at the University of Liverpool. His research interests include power electronics, advanced control theory and DSP-based control applications.

Dr. Hornik is a member of The Institution of Engineering and Technology (IET).

Qing-Chang Zhong (M'04–SM'04) received the Diploma degree in electrical engineering from Hunan Institute of Engineering, Xiangtan, China, in 1990, the M.Sc. degree in electrical engineering from Hunan University, Changsha, China, in 1997, the Ph.D. degree in control theory and engineering from Shanghai Jiao Tong University, Shanghai, China, in 1999, and the Ph.D. degree in control and power engineering from Imperial College London, London, U.K., in 2004.

He was with Technion—Israel Institute of Technology, Haifa, Israel; Imperial College London, London, U.K.; University of Glamorgan, Cardiff, U.K.; and the University of Liverpool, Liverpool, U.K. Since August 2010, he has been with the Department of Aeronautical & Automotive Engineering, Loughborough University, Leicestershire, U.K., as a Professor of control engineering. He is the author or coauthor of three research monographs: *Robust Control of Time-Delay System*s (Springer-Verlag, 2006), *Control of Integral Processes With Dead Time* (Springer-Verlag, 2010), *Control of Power Inverters for Distributed Generation and Renewable Energy* (Wiley-IEEE Press, scheduled to appear in 2011). His current research interests include robust and H-infinity control, time-delay systems, process control, power electronics, electric drives and electric vehicles, distributed generation, and renewable energy.

Prof. Zhong is a Fellow of The Institution of Engineering and Technology (formerly, the Institution of Electrical Engineers) and was a Senior Research Fellow of the Royal Academy of Engineering/Leverhulme Trust, U.K. (2009–2010). He is a recipient of the Best Doctoral Thesis Prize at Imperial College London.